Extraction of Coherent Structures from Natural and Actuated Flows

Jens Kasten, Tino Weinkauf, Christoph Petz, Ingrid Hotz, Bernd R. Noack, and Hans-Christian Hege

Abstract We present feature-extraction techniques for numerical and experimental data of complex fluid flows. Focus is placed on efficient analysis and visualization of coherent structures of snapshots, temporal evolution and parameter-dependency of coherent structures. One key enabler are Galilean invariant flow quantities based on pressure, acceleration, vorticity and velocity Jacobians. Other important catalyzers are Lagrangian filters that distill persistent strong particle-fixed features while neglecting weak and short-living ones. The proposed feature extraction framework is exemplified for the time-dependent natural and actuated flow around a high-lift airfoil, as well as other benchmark configurations of the SFB 557.

1 Introduction

Fluid flow datasets arising from experiments and simulation increase in size and complexity. The automated analysis of numerically given fluid data therefore becomes more and more important. During the past two decades, much effort has been devoted to the development of computer graphical techniques for display of steady and unsteady flow fields – both in 2D and 3D. The resulting tools are widely used today for visualization of flow fields. However, analyzing and understanding intricate flow structures is often difficult — even with advanced visualization tools, since only *raw data* are displayed instead of the more interesting *flow structures*.

Researchers and practitioners are interested in the main flow characteristics that are relevant for their specific analysis questions. Schlichting's book 'Boundary layer theory' [18] and the Journal of Fluid Mechanics contain many masterpieces of hand-crafted principle flow sketches — revealing the main flow characteristics in a single

Jens Kasten, Christoph Petz, Ingrid Hotz, Hans-Christian Hege
Zuse Institute Berlin (ZIB), Takustr. 7, 14195 Berlin, Germany

Tino Weinkauf
Courant Institute of Mathematical Sciences, 715 Broadway, New York, NY 10003, USA

Bernd R. Noack
Institut Pprime, CNRS Université de Poitiers ENSMA, CEAT, 43 rue de l'aérodrome, F-86036 Poitiers cedex, France

picture. The goal of our work is to advance analysis and visualization techniques to a stage where similarly insightful features can be distilled from raw data in a semi-automatic or even automatic manner.

In visual data analysis such flow structures are often called *'features'*. A feature, as used in this paper, is a mathematically defined geometric object (point, line, surface, volume) that potentially is time-dependent and represents some important flow structure, e.g., a stagnation point, vortex core line, or vortex region. Though experts in fluid dynamics have intuitive conceptions of specific flow features, unique and agreed mathematical characterizations are often missing. Even for the concept of a 'vortex' there is no generally accepted mathematical definition. Identifying practically interesting flow structures and finding mathematical definitions therefore is part of the research. If such a mathematical characterization is given, often it is non-trivial to extract the corresponding structures algorithmically. The development of efficient and robust algorithms for feature extraction therefore is another task.

Once such features have been extracted and are represented as geometric objects, they can be used in many ways. Here, we are mainly interested in using them for creation of visualizations that *provide insight*. Development of perceptually effective feature visualizations therefore is also part of the research.

Feature-based visualization ideally distills information which conveys (i) the coherent structures, (ii) the temporal evolution of these structures, and (iii) the structural changes due to variation of configuration parameters (configuration robustness). Furthermore, it reduces the amount of information, allowing to focus on specific aspects of the flow and providing interactive exploration.

In this paper we present a short overview of feature extraction techniques that we have developed during recent years in the framework of the SFB 557, putting special emphasis on recently developed methods. Due to space limitations we do not try to present recent developments of other groups. A more complete overview over the field can be found, for example, in references [12] and [17].

After introducing basic mathematical concepts (Sect. 2.1), we discuss feature extraction algorithms for steady flows (Sect. 2.2) and unsteady flows (Sect. 2.3). Then we present some selected techniques for discrete feature extraction (Sect. 2.4) and show some applications to actuated flows (Sect. 3). Finally, we discuss the results and draw some general conclusions (Sect. 4).

2 Feature Extraction

2.1 Fundamental Concepts

Notation. We consider either steady flows in a spatial domain $D = \Omega \subset \mathbb{R}^n$ ($n = 2,3$) or unsteady flows in a spatiotemporal domain $D = \Omega \times [0,T]$. A flow is specified by physical fields on domain D. For incompressible flows the phase space is completely specified by velocity $\mathbf{v} : D \to \mathbb{R}^n$ and pressure $p : D \to \mathbb{R}$. These fields are typically discretely sampled in D.

Features. Features may either be directly based on the given flow, or on derived scalar, vector or tensor fields. Examples of derived scalar fields are the Okubo-Weiss field Q and the λ_2 field. Here, Q is $\frac{1}{2}(||A||^2 - ||S||^2)$ (with $A = \frac{1}{2}(\nabla \mathbf{v} - (\nabla \mathbf{v})^T)$ and $S = \frac{1}{2}(\nabla \mathbf{v} + (\nabla \mathbf{v})^T)$). λ_2 is the second eigenvalue of the symmetric matrix $A^2 + S^2$. A frequently used derived vector field is vorticity $\omega = \nabla \times \mathbf{v}$. Considering common feature definitions, there are two re-occurring concepts, namely ridge lines and scalar/vector field topology, which will be recalled in the following.

Typical features of a ***scalar field*** f are, e.g., *minima, maxima, saddle points, ridge* and *valley lines*. Ridges and valleys, as extremal structures, play a special role in flow analysis. The concept of extremal structures has been studied by Eberly [1] and Lindeberg [8] in great generality. Here we are mainly interested in one-dimensional ridge lines, which are defined as follows: For a smooth function $f : U \to \mathbb{R}$ of an open set $U \subset \mathbb{R}^n$ let $\nabla_{\mathbf{x}_0} f = g$ be the derivative of f at $\mathbf{x}_0 \in U$ and $H_{\mathbf{x}_0}(f) = H$ the Hessian of f at $\mathbf{x}_0$. Further let $\lambda_1, \lambda_2, \ldots, \lambda_n$ be the sorted eigenvalues of the Hessian matrix and $e_1, e_2, \ldots, e_n$ the corresponding unit eigenvectors. Then, a point x_0 is defined as a *ridge point*, if $\lambda_{n-1} < 0$ and $\nabla_{\mathbf{x}_0} f \cdot \mathbf{e}_i = 0$ for $i = 1, 2, \ldots, n-1$. A *valley point* is a ridge point in the negative field $-f$.

Typical features of a ***vector field*** $\mathbf{v}$ are *integral curves* (e.g., streamlines or pathlines), or components of *flow topology*, i.e., *critical points* $\mathbf{x}_c$ with $\mathbf{v}(\mathbf{x}_c) = 0$, *1D-separatices* (= streamlines starting in a saddle point in direction of their eigenvector corresponding to the unique negative or positive eigenvalue), and *2D-separatices* (= stream surfaces starting in a saddle point in the plane spanned by the two eigenvectors with matching sign).

For scalar fields f, also ***scalar topology*** is considered, which is the flow topology of the gradient vector field ∇f. The existence of a potential gives additional structure to this topology, and it can be described with more ease, as no closed integral lines (limit cycles) can occur. The so-called *Morse-Smale complex* of a real-valued field partitions its domain into regions having uniform gradient flow behavior.

For a successful feature extraction, not only an appropriate feature definition, but also efficient and stable extraction algorithms are essential. Thereby, we differentiate *discrete algorithms*, which work directly with sampled data, and *continuous algorithms*, which require spatial or spatiotemporal interpolation.

2.2 Algorithms for Steady Data

We start with feature extraction methods originally developed for steady flow fields. Typically, these methods are related to streamline analysis.

Streamline-based Topology. Topological methods segment a flow field into sectors of equivalent streamline behavior by extracting critical points, separation lines and surfaces (see e.g. [23]). They are especially well suited for the analysis of flow separation. For complex 3D topologies, these separating surfaces tend to hide each other as well as other topological features. To solve this problem, the concept of

saddle connectors and boundary switch connectors has been introduced [21; 27; 23]. The main idea is to replace stream surfaces by their intersection curves, which are particular streamlines. The visualization of saddle connectors instead of the separation surfaces results in expressive visualizations even for topologically complex data sets. In addition, the integration of stream surfaces is computationally more involved and less stable than the integration of streamlines, since convergence and divergence effects on the stream surface may occur.

Vortex Related Features. Complementing the topological analysis, vortices and vortex systems are the most prominent features in fluid flows. Both, the regions of influence of vortices – called vortex regions – and the locations of the vortex centers (in 2D) or center lines (in 3D) are of interest. Since, there are several characterizations of vortices, there is a wide range of algorithms to extract these. For an overview see Post et al. [13].

Vortex and Strain Skeletons Based on Scalar Identifiers. While vortex region quantities are Galilean invariant, many methods for extracting vortex cores are based on streamline analysis and thus depend on the frame of reference. Alternative approaches to extract vortex cores use Galilean invariant vortex region quantities. Besides displaying these scalar quantities (such as Okubo-Weiss and λ_2) directly, *extremum lines* of the scalar fields represent vortex cores explicitly as line type features. We developed methods for their extraction based on the notion of ridges [15] and the notion of watersheds/topology [16]. For the visualization of extracted line features, an iconic representation indicating their scale and extent is used. In Section 2.4 we present two novel methods based on discrete topology that aim at extracting extremal lines in a robust manner.

Hierarchical Vortex Regions. We have further complemented this set of methods by a scheme for extracting regions around a vortex core [11]. Vortex systems often consist of a spatial hierarchy of nested vortices. In this 2D streamline-based technique, a vortex region is defined by surrounding lines that intersect the velocity field in an constant angle along the lines. Clusters of homotopic lines around vortex centers define a vortex region. These regions build a spatial hierarchy of vortex regions, cf. Fig. 8. Vortex splitting and merging events can be detected and visualized with this technique.

2.3 Algorithms for Unsteady Data

Principally, all methods for steady flow fields can be applied to single time steps of unsteady fields. A framework to track the temporal development of extracted structures has been developed by introducing feature flow fields [22], which was applied to topological structures as well as vortex cores [20]. Treating time as additional parameter was proposed in [28] to extract topological changes over time. While providing some interesting insight, these so-called snapshot features are not sufficient for a complete analysis of unsteady data. Most flow phenomena are unsteady in

nature and particle motion is described by *pathlines*. This generally leads to different flow patterns. The topological concept has been extended to a pathline oriented topological segmentation for periodic 2D time-dependent vector fields [19]. The approach detects critical pathlines as well as basins from which the pathlines converge to the critical ones. In the following, we describe three methods especially designed for time-dependent flows based on the analysis of pathlines.

Vortex Core Detection based on Swirling Motion. One way to assess vortices in experiments is to emit particles (smoke) into the flow and to examine their behavior: patterns of swirling flow indicate vortices. For steady numerical and measured datasets, Peikert and Roth formulated the successful concept of the 'parallel vectors' operator and presented a fast and robust extraction technique [9]. We have extended this concept to extract the cores of swirling particle motion in unsteady flows based on the behavior of pathlines [26].

Given a time-dependent vector field $\mathbf{v}(\mathbf{x},t)$, we consider the dynamic system $\frac{d}{dt}(\mathbf{x},t)^T = (\mathbf{v}(\mathbf{x},t),1)^T$ by including time as an explicit state variable at the expense of an increase in dimension by one. Pathlines then are tangent curves of the vector field $\mathbf{p}(\mathbf{x},t) = (\mathbf{v}(\mathbf{x},t),1)^T$. In the 3D unsteady setting, the Jacobian $\mathbf{J}(\mathbf{p})$ has the eigenvalues $e_1, e_2, e_3, 0$ with the respective four eigenvectors $(\mathbf{e}_1,0)^T$, $(\mathbf{e}_2,0)^T$, $(\mathbf{e}_3,0)^T$, $\mathbf{f}$, where $\mathbf{e}_1, \mathbf{e}_2, \mathbf{e}_3$ are the eigenvectors of the spatial Jacobian. Under the condition that $\mathbf{J}(\mathbf{p})$ has a pair of conjugate complex eigenvalues (sorted such that e_1, e_2 are complex and e_3 is real), we find swirling motion around the point of interest which is a necessary condition for a swirling particle core. As we have shown in [26], a point $\mathbf{x}$ is *on* the swirling particle core if the flow vector $\mathbf{p}(\mathbf{x})$ lies in the plane of non-swirling flow spanned by the two real eigenvectors $\mathbf{e}^s := (\mathbf{e}_3,0)^T$ and $\mathbf{f}$. In other words, the swirling particle cores are at locations where

$$\lambda_1\mathbf{p} + \lambda_2\mathbf{e}^s + \lambda_3\mathbf{f} = \mathbf{0} \quad \text{with} \quad \lambda_1^2 + \lambda_2^2 + \lambda_3^2 > 0\,, \tag{1}$$

i.e. where the 4D vectors $\mathbf{p}$, $\mathbf{e}^s$ and $\mathbf{f}$ are coplanar. The resulting core structures are lines sweeping over time, i.e., surfaces in the space-time domain. At a single time step, particles group around these core lines forming patterns of swirling motion. In order to extract them, we have shown how to re-formulate the problem using the parallel vectors operator [9] and applying it accordingly. Fig. 1 shows the extraction result for a flow behind a cylinder.

Finite-time Topology. Critical points of the velocity field, the basic building blocks of vector field topology, are not Galilean invariant. If no preferred frame of reference is given, topological analysis appears somewhat arbitrary. Acceleration $\mathbf{a}(\mathbf{x},t) = \partial_t\mathbf{v}(\mathbf{x},t) + (\mathbf{v}(\mathbf{x},t)\cdot\nabla)\,\mathbf{v}(\mathbf{x},t)$, however, is a Galilean invariant property. In steady fields, particles at fixed points have zero acceleration; in unsteady fields acceleration at these points is small compared to their neighborhoods. Therefore, particles with minimal acceleration $\|\mathbf{a}\|$ are of interest. We call space-time points $(\mathbf{x}_0,t_0)$ where $\|\mathbf{a}(\mathbf{x}_0,t_0)\|$ has a local minimum in space *Lagrangian equilibrium points* (LEP).

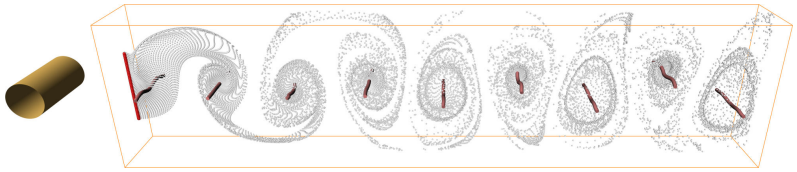

Fig. 1: 3D unsteady flow behind a cylinder. The red lines denote swirling particle cores at a certain time step. The gray fluid particles show that the core lines are located at the centers of swirling particle motion.

Fluid dynamicists are interested in the dominant structures that influence the flow behavior. Of particular interest are long-living features. We take a Lagrangian view by considering trajectories ('particles') in space-time domain D and observing their properties. By measuring how much and how long particles exhibit characteristic properties, we can filter out salient, long-living structures. Let $\mathbf{p}(t;\mathbf{x}_0,t_0)$ be the trajectory of a particle moving through point $\mathbf{x}_0$ at time t_0. As mentioned before, an interesting feature is 'low acceleration magnitude' $a(\mathbf{x},t) = \|\mathbf{a}(\mathbf{x},t)\|$. To evaluate this, we compute the average of a^2 for particles moving through point $\mathbf{x}_0$ at time t_0

$$\mathscr{A}(\mathbf{x}_0,t_0) = \frac{1}{t_{\max}(\mathbf{x}_0,t_0) - t_{\min}(\mathbf{x}_0,t_0)} \int_{t_{\min}(\mathbf{x}_0,t_0)}^{t_{\max}(\mathbf{x}_0,t_0)} a\left(\mathbf{p}(t;\mathbf{x}_0,t_0),t\right)^2 dt \qquad (2)$$

over some time span $[t_{\min}(\mathbf{x}_0,t_0), t_{\max}(\mathbf{x}_0,t_0)] \subseteq [t_0-\tau, t_0+\tau]$ with maximal width 2τ. The actual width is called 'feature lifetime'. The parameters $t_{\min}$ and $t_{\max}$ are chosen such that along the pathline segment $\{\mathbf{p}(t;\mathbf{x}_0,t_0) \mid t \in [t_{\min}, t_{\max}]\}$ two condi-

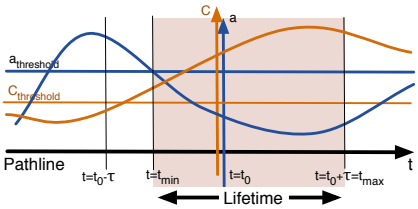

Fig. 2: Definition of a feature's lifetime along a pathline (parametrized by time). In the depicted case parameter $t_{\min}$ is determined by the acceleration threshold and $t_{\max}$ by the maximum lifetime window.

tions are fulfilled (cf. Fig. 2): (i) the acceleration magnitude a is below some threshold $a_{\text{threshold}}$ and (ii) the difference between the average acceleration at spatially neighbored grid points and the acceleration at the considered points (denoted as C_{a}) is greater then some threshold $C_{\text{threshold}}$:

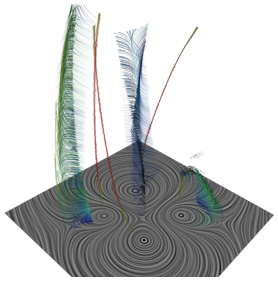

Fig. 3: Mixing of six Oseen vortices. The time axis is orthogonal to the texture plane. The illuminated pathline segments indicate the lifetime interval $[t_{\max}, t_{\min}]$. *(magnify the image)*

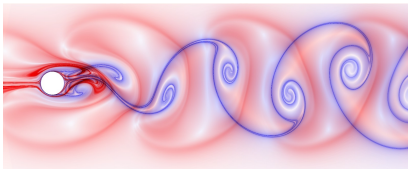

Fig. 4: Dataset of the flow behind a circular cylinder. Depicted is the simultaneous visualization of forward (red) and backward (blue) L-FTLE , integration time $T = 3$ periods.

$$
\begin{aligned}
t_{\min}(\mathbf{x}_0, t_0) = \min(t' \in [t_0 - \tau, t_0] \mid \forall t \in [t', t_0] : \\
a(\mathbf{p}(t; \mathbf{x}_0, t_0), t) < a_{\text{threshold}} \text{ and} \\
C_{\text{a}}(\mathbf{p}(t; \mathbf{x}_0, t_0), t_0) > C_{\text{threshold}}),
\end{aligned} \tag{3}
$$

and $t_{\max}$ equivalently. In the resulting field $\mathscr{A}$ the minima are searched (due to the averaging these are not exactly the LEPs). These minima are then filtered by a lifetime criterion $t_{\max}(\mathbf{x}_0, t_0) - t_{\min}(\mathbf{x}_0, t_0) > t_{\text{threshold}}$.

As an example, the mixing of six Oseen vortices in 2D is depicted in Fig. 3. The lifetime and averaged squared acceleration $\mathscr{A}$ were computed; then the minima of $\mathscr{A}$ were determined and used as seed points for pathlines. Length and color coding of the pathlines indicate the lifetime. Since particles remain a long time in the vicinity of vortices, this approach is useful for extraction of time-dependent vortex cores.

Localized Finite-time Lyapunov Exponent. The Finite-Time Lyapunov Exponent (FTLE) is a measure for the rate of separation of particles in time-dependent flow fields. FTLE is typically computed by analyzing the flowmap, which maps the end points of pathlines to their starting positions. The spectral norm of the gradient of this map determines the separation of a pathline over a finite period of time. The gradient is in general approximated using finite differences. To obtain a measure for the convergence of particles, the flowmap has just to be computed for particles traced backwards in time.

This standard approach assumes a linearization of the flow, which is only valid for short advection times. Furthermore, the sampling distance of the pathlines has a strong impact on the results: Large values lead to wrong results, since the particles more and more diverge from the trajectory for which the FTLE is to be measured. One remedy is a continuous renormalization of the pathlines.

In [7] we presented an algorithm for measuring the separation by tracing a single pathline. We use the Jacobian matrix as a generator of the separation to measure it locally. Consider a pathline $\mathbf{p}(t) = \mathbf{p}(\mathbf{x}_0, t_0, t)$ for a particle started at space-time location $(\mathbf{x}_0, t_0)$. The deviation of trajectories of infinitesimally close particles started at $(\mathbf{x}_0 + \delta_0, t_0)$, with $\delta_0 \to 0$, are governed by the Jacobian of the velocity field along $\mathbf{p}(t)$. The time evolution of the deviation in a flow field $\mathbf{v}$ is given by the differential equation

$$\dot{\delta}(t) = (\nabla \mathbf{v}|_{\mathbf{p}(t)})\delta(t), \tag{4}$$

with $\delta(0) = \delta_0$. For sufficiently small values of $t < \Delta_t$, the gradient can be approximated by the constant matrix $\nabla_0 = \nabla \mathbf{v}|_{\mathbf{p}(0)}$. Solving the differential equation then yields $\delta(t) = \exp(\nabla_0\, t)\delta_0$. By discretizing the total integration time T in intervals of size Δ_t, a repeated application of the previous expression results in $\delta(T) = \left(\prod_{i=N-1}^{0} \exp(\nabla_i\, \Delta_t)\right) \delta_0$, where N is the number of discretized time steps, $N \cdot \Delta_t = T$ and $\nabla_i = \nabla \mathbf{v}|_{\mathbf{p}(i\Delta_t)}$. Thus, the matrix

$$\Psi_T(\mathbf{p}) = \left(\prod_{i=N-1}^{0} \exp(\nabla_i \Delta_t) \right) \tag{5}$$

is an approximate mapping of the neighborhood at the starting point $\mathbf{p}(0)$ to deviations at the end point $\mathbf{p}(T)$ after advection, similar to the flowmap gradient. The 'localized FTLE' defined by

$$\text{L-FTLE}^{+}(\mathbf{x}_0, t_0, T) = \frac{1}{T} \ln(||\Psi_T(\mathbf{p}(\mathbf{x}_0, t_0, .)||_\lambda) \tag{6}$$

reflects the separating behavior of infinitesimally close particles along the pathline. Analogously, the exponent L-FLTE^{-} for backward integration is defined, describing the convergence behavior.

In Fig. 4, for a 2D instationary flow behind a circular cylinder the L-FTLE is computed for three shedding periods, showing the typical pattern of the von-Kármán vortex street. The separation and convergence of particles is illustrated by red and blue coloring, respectively. The time-dependent Lagrangian structures emerge clearly.

2.4 Discrete Feature Extraction

In this section, we present two methods for the extraction of extremal lines using scalar field topology. Due to its robustness, we use the characterization of the topological skeleton as a Morse-Smale (MS) graph on a discrete domain as introduced by Forman [4]. In this context, the grid underlying the discretized scalar field is considered as a simplicial complex. In the simplicial graph, every node corresponds to a simplex in the simplicial complex and the links represent the neighborhood of these simplices. In two dimensions, there are three types of critical points, which are nodes in the simplicial graph: minima (0-cells or vertex nodes), saddles (1-cells or edge nodes) and maxima (2-cells or face nodes). The setting is analog in three

dimensions, but the saddles split up into two types: 1-saddles and 2-saddles. In this topological setting, extremal lines are found as separatrices of the MS complex, which are discrete integral lines connecting critical points. Since we are typically interested in the minimal lines of the scalar field, the connecting lines of the 0-1 edges represent the *raw feature set* of interest.

A common problem with topological methods is their sensitivity to noise: every local extremum of the scalar field is a critical point (often referred to as "oversegmentation"). *Topological simplification* aims at reducing this complexity by successively removing pairs of critical points (*cancellation*) in an order determined by some importance measure. The result is still a valid MS complex, but with less critical points.

As a measure of importance, we use *persistence*, introduced by Edelsbrunner et al. [3; 2]: critical points with lower persistence will be removed before those with higher persistence. Loosely speaking, persistence measures how long connected components of an isocontour exist when the isovalue is increased. More precisely, persistence measures the function value difference between acts of creation (minima and splits at saddles) and acts of destruction (maxima and merges at saddles).

After this brief introduction into MS simplification, we will now discuss specific problems: for 2D, we introduce an extension of the concept of persistence to separatrices, and for 3D, we deal with technical problems of the MS simplification process.

Separatrix Persistence. Persistence was originally introduced for critical points. Thus, only 0-dimensional features of the topological skeleton could be organized into a hierarchy. In two dimensions, the 1-dimensional features, the separatrices, are of intereset, too. In order to measure the importance of separatrices, we propose *separatrix persistence* [24]: Let $\mathbf{s}$ denote a saddle connected to the minima $\mathbf{m}_i$ and maxima $\mathbf{M}_i$ in the skeleton of the scalar field f. The *persistence of a separatrix* ℓ is defined for each point $\mathbf{x} \in \ell$ as

$$p_\ell(\mathbf{x}) = \begin{cases} f(\mathbf{x}) - \max(f(\mathbf{m}_i)) \ , & \text{if } \ell \text{ is a maximal line} \\ \min(f(\mathbf{M}_i)) - f(\mathbf{x}) \ , & \text{if } \ell \text{ is a minimal line.} \end{cases} \tag{7}$$

Separatrix persistence measures the significance of every point on a separatrix. As

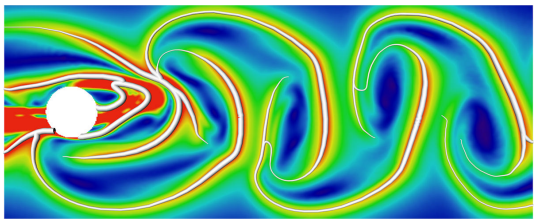

Fig. 5: Flow behind a cylinder. Maximal lines of forward L-FTLE, extracted using discrete topology, are shown in gray. Their thickness is scaled according to their separatrix persistence.

it is derived from classical persistence, it inherits the stability under small perturbations. Obviously, p_ℓ reaches its highest value at the extremum. The point on ℓ with the lowest persistence is the saddle **s**. Separatrix persistence allows us to identify the most important, most salient parts of all separatrices contained within a MS complex. Fig. 5 shows an example at a flow behind a cylinder.

Discrete Feature Extraction in 3D. In theory, the cancellation of critical points extends from 2D to 3D without significant changes. But in praxis there evolve some problems concerning the implementation as well as the results. First, this makes an adaptation of the cancellation process necessary and, moreover, calls for an additional post processing filtering step, which will be described in the following.

Extracting the extremal skeleton. The direct implementation of the cancellation algorithm in 3D leads to two problems due to the additional saddle connectors. First, the generation of multiple connections between saddles causes a memory problem. To ease this problem we adapted the concept of *valences* (number of links per node in the MS complex) introduced by Gyulassy [5]: Cancellation in the 1-2 layer is only performed if the number of new edges falls below some predefined thresholds. Furthermore, multiple edges between two vertices of the MS complex are stored only once. The multiplicity of those edges is counted in the edge data structure.

Second, the 1-2 connections get knotty which limits the cancellation possibilities. These knotty structures remain at all persistence levels and generate a complex skeleton of minima lines. Furthermore, these knots complicate the cancellation algorithm. The cancellation in three dimensions is a non-deterministic polynomial-time (NP) hard problem. Thus, for large data sets only heuristics can be applied.

Filtering. For filtering the discrete extremal structures, we use a quantity that measures for each point in the domain of a scalar field the local 'rigdeness'. In their work using the parallel vectors operator, Peikert and Sadlo [10] extract a set of raw feature points using the ridge condition for a scalar field f: $Hg = \lambda g$, or equivalently $\frac{(Hg,g)}{\|Hg\|\|g\|} = 1$. Measuring at a point $\mathbf{x}_0 \in \Omega$ to which extend $g(\mathbf{x}_0) := \nabla_{\mathbf{x}_0} f$ and $H_{\mathbf{x}_0}(f)\nabla_{\mathbf{x}_0} f = H_{\mathbf{x}_0} g(\mathbf{x}_0)$ are parallel, we define the *'ridgeness'* $R(f)$:

$$R(f)(\mathbf{x}_0) = \frac{(H_{\mathbf{x}_0}(f)\, g(\mathbf{x}_0)\,,\, g(\mathbf{x}_0))}{\|H_{\mathbf{x}_0} g(\mathbf{x}_0)\|\, \|g(\mathbf{x}_0)\|} \quad .$$

This measure, applied to the results of the first step, suffices for filtering discrete extremal structures.

Application. As an example, we consider a flow field behind a circular cylinder. The λ_2 measure is used as an indicator for vortices. In Fig. 6(a), the raw feature skeleton resulting from the MS cancellation can be seen. The lines are color-coded with λ_2. Fig. 6(b) shows the filtering with λ_2 itself. By removing every second point from the lines, a line of best fit is computed from the discrete lines, which run along the grid. The lines are scaled with negative values of λ_2. The isosurfaces of λ_2 separate most parts of the lines from uninteresting structures – the vortex core lines remain. On the other side, directly behind the cylinder, the structures cannot be distinguished from

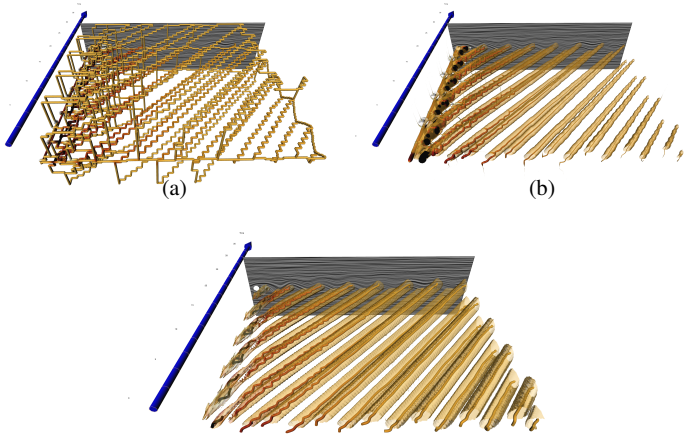

Fig. 6: Time-dependent vortex core lines of a flow behind a circular cylinder. The blue arrow is the time axis. As vortex-indicating quantity λ_2 has been chosen. The lines were computed with a discrete method that extracts extremal structures (a) and then filtered with λ_2 (b) as well as with ridgeness (c). The tube-like semi-transparent surfaces are isosurfaces of λ_2 and ridgeness. The lines (clearly visible only with magnification) are colored according to λ_2.

each other and are still linked at some points. Thus, we use ridgeness as another filter criterion, cf. Fig. 6(c). Here, the isosurfaces of high ridgeness separate the lines much better.

3 Features of Actuated Flows – Results

In this section, we present some results of our methods applied to a more complex configuration, the Swept Constant Chord Half-model (SCCH) [25], cf. Fig. 7, with flow actuation. The time-dependent, three-dimensional CFD-datasets show the sim-

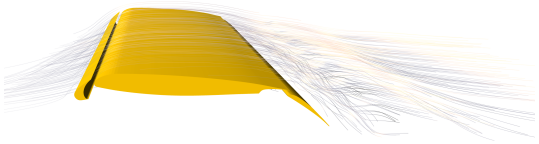

Fig. 7: Snapshot visualization of the flow around an airfoil. Illuminated streamlines illustrate the actuated flow. *(magnify the image)*

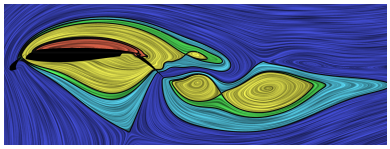

Fig. 8: Hierarchical vortex regions of the flow around an airfoil (SCCH) in a plane, after subtracting the average flow. *(magnify the image)*

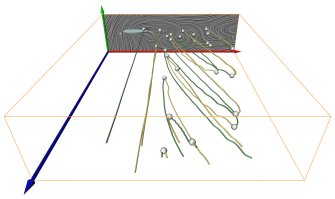

Fig. 9: Tracking of critical points for a two-dimensional instationary version of the airfoil dataset. *(magnify the image 5-6 times)*

ulated flow around an airfoil for different configurations of actuation.

First, for one actuation state of the model, we extract the hierarchy of vortex regions. After choosing an appropriate frame of reference by subtracting the average flow of the field, the vortices behind the airfoil get clearly visible in the line integral convolution (LIC) texture. Applying hierarchical vortex extraction, cf. Fig. 8, the pairing of vortices directly behind the airfoil is clearly highlighted.

For a time-dependent analysis, first we apply our tracking method to a two-dimensional instationary dataset of the SCCH model. In Fig. 9, this result is displayed (red and green axes = spatial dimensions, blue axis = time). A snapshot of the flow is depicted in one LIC plane together with the critical points (gray spheres) of that time step. They serve together with fold bifurcations (births and deaths of critical points depicted as gray spheres in the spatiotemporal volume) as the starting points of the tracking. The yellow lines indicate the tracking of saddles and the green lines the center lines of vortices.

(a) (b)

Fig. 10: L-FTLE$^-$ for two versions of the SCCH dataset - non-actuated (a) and actuated (b). The effect of the actuation parameter can be clearly seen. *(magnify the images)*

In Fig. 10, the localized finite-time Lyapunov exponent (L-FTLE) is calculated for two versions of the SCCH dataset – non-actuated (a) and actuated (b). It provides provides insight into the complex nature of instationary parameter-dependent flows. Here, it is computed in backwards direction and, hence, shows the convergence of particles. The time-dependent vortices thus can be clearly seen. Furthermore, it is possible to observe the effect of the actuation. The vortex pairing behind the airfoil is not as strong in the actuated version as in the non-actuated one.

In [25] (cf. also [14]), we studied the influence of the actuation parameters frequency and intensity of air injection on vortex structures and thereby, e.g., on lift. We showed, (i) how vortex structures change when actuation parameters are varied, (ii) when vortex structures are leading to more favorable situations (e.g. higher lift), and (iii) when new, detrimental vortex structures are introduced by the flow control itself. This analysis demonstrates that feature-based analysis and visualization supports the understanding of the physics behind flow actuation.

4 Discussion and Conclusion

Visualization and feature extraction comprises an astonishingly rich expertise in data analysis and is at an advanced stage in many scientific areas. In fluid dynamics, visualization has its roots in experimental techniques and therefore has a long tradition. Computer-based methods, however, offer more opportunities, particularly regarding the extraction and visual accentuation of flow *structures* or flow *features*.

Regarding steady 2D flows, powerful methods for visual analysis are already available. Our aim was to significantly contribute to the extension of methods to deal with 3D, unsteady and parameter-dependent flows, cf. Fig. 11 and Fig. 12.

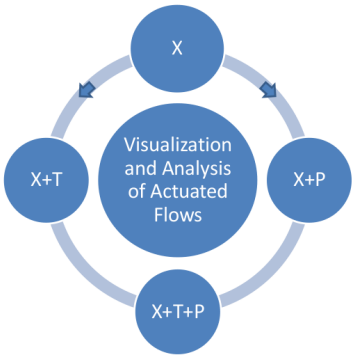

Fig. 11: Parameter dependencies of flow data sets: steady flows X, unsteady flows X+T, parameter dependent steady and unsteady flows X+P and X+T+P, resp.

Method	X	X+P	X+T	X+T+P
Streamline-based Topology [21; 27] [22; 28]	u	u	u	u
Vortex Core Lines (Ridges) [15; 16]	u	t	u	t
Vortex Core Lines (Swirl) [20; 26]	u	t	u	t
Hier. Vortex Regions [11]	u	u	t	t
FTT [6]			u	t
L-FTLE [7]			u	u

Fig. 12: Methods for feature extraction developed by the authors for the four cases of parameter dependencies depicted in Fig. 11. u: the method was used for this case; t: the method is transferable to this case.

With this generalization two major challenges are associated. First, the transition from 2D to 3D which confronts us with significantly more complex flow structures; this requires the development of suitable filtering criteria that select the really important structures. Second, the transition from steady to unsteady flows requires a switch in perspective: tracking of features in snapshots can reveal interesting information, but is not sufficient; considering pathlines instead of streamlines is another step and changing to a Lagrangian viewpoint instead of an Eulerian is a third one.

We tackled these problems as follows (cf. Fig. 12): First, we developed feature extraction methods based on pathlines. These are pathline-based topology, also in combination with Galileian-invariant variables like acceleration, extraction of vortex structures based on detection of swirling motion characteristics, as well as Lagrangian analysis techniques based on FTLE. Second, we developed and adapted discrete methods to flow analysis problems, which particularly provide controlled simplification. Additionally, we introduced techniques that utilize lifetime parameters for filtering in continuous extraction methods.

The developed techniques have been successfully applied to benchmark configurations of the collaborative research center SFB 557. We demonstrated that the feature extraction and visualization techniques aid researchers in understanding natural and actuated flows.

Our flow visualizations have been awarded by the fluid dynamics community, adopted for book covers, illustrate popular science magazines and were used for many other similar purposes. Thereby, we contributed also to the outreach activities of SFB 557.

Acknowledgements The project is part of the DFG SFB 557 "Control of complex turbulent shear flows"; it is also supported by the Emmy Noether program of DFG. All visualizations have been created using Amira - a system for advanced visual data analysis (http://amira.zib.de).

References

[1] Eberly, D.: Ridges in Image and Data Analysis. Kluwer Acadamic Publishers, Dordrecht (1996)

[2] Edelsbrunner, H., Harer, J., Natarajan, V., Pascucci, V.: Morse-smale complexes for piecewise linear 3-manifolds. In: Proc. 19th Sympos. Comput. Geom. 2003, pp. 361 – 370 (2003)

[3] Edelsbrunner, H., Letscher, D., Zomorodian, A.: Topological persistence and simplification. Discrete and Computational Geometry **28**, 511 – 533 (2002)

[4] Forman, R.: Morse theory for cell-complexes. Advances in Mathematics **134**, 90–145 (1998)

[5] Gyulassy, A.: Combinatorial Construction of Morse-Smale Complexes for Data Analysis and Visualization. Ph.D. thesis, University of California, Davis (2008)

[6] Kasten, J., Hotz, I., Noack, B., Hege, H.C.: On the extraction of long-living features in unsteady fluid flows. In: TopoInVis 2009, Springer, to appear 2010

[7] Kasten, J., Petz, C., Hotz, I., Noack, B., Hege, H.C.: Localized finite-time Lyapunov exponent for unsteady flow analysis. In: Proc. Vision Modeling and Visualization (VMV), pp. 265 – 274 (2009)

[8] Lindeberg, T.: Edge detection and ridge detection with automatic scale selection. International Journal of Computer Vision **30(2)**, 117–156 (1998)

[9] Peikert, R., Roth, M.: The parallel vectors operator - a vector field visualization primitive. In: Proc. IEEE Visualization 99, pp. 263–270 (1999)

[10] Peikert, R., Sadlo, F.: Height Ridge Computation and Filtering for Visualization. In: IEEE Pacific Visualization Symposium 2008, pp. 119 – 126 (2008)

[11] Petz, C., Kasten, J., Prohaska, S., Hege, H.C.: Hierarchical vortex regions in swirling flow. Computer Graphics Forum **28**, 863–870 (2009)
[12] Pobitzer, A., Peikert, R., Fuchs, R., Schindler, B., Kuhn, A., Theisel, H., Matković, K., Hauser, H.: On the way towards topology-based visualization of unsteady flow – the state of the art. Computer Graphics Forum (2010), Proc. Eurographics 2010, to appear
[13] Post, F., Vrolijk, B., Hauser, H., Laramee, R., Doleisch, H.: Feature extraction and visualisation of flow fields. In: Proc. Eurographics 2002, State of the Art Reports, pp. 69–100 (2002)
[14] Sahner, J.: Extraction of vortex structures in 3d flow fields. Ph.D. thesis, Zuse Institute Berlin and Univ. Magdeburg, Fakultät für Informatik (2009)
[15] Sahner, J., Weinkauf, T., Hege, H.C.: Galilean invariant extraction and iconic representation of vortex core lines. In: K. Brodlie, K.J., D. Duke (ed.) Proc. Eurographics / IEEE VGTC Symposium on Visualization (EuroVis '05), pp. 151–160, Leeds, UK (2005)
[16] Sahner, J., Weinkauf, T., Teuber, N., Hege, H.C.: Vortex and strain skeletons in Eulerian and Lagrangian frames. IEEE Transactions on Visualization and Computer Graphics **13**, 980–990 (2007)
[17] Salzbrunn, T., Jänicke, H., Wischgoll, T., Scheuermann, G.: The state of the art in flow visualization: Partition-based techniques. In: SimVis, pp. 75–92 (2008)
[18] Schlichting, H.: Boundary-Layer Theory. McGraw-Hill (1979)
[19] Shi, K., Theisel, H., Weinkauf, T., Hauser, H., Hege, H.C., Seidel, H.P.: Path line oriented topology for periodic 2D time-dependent vector fields. In: Proc. Eurographics / IEEE VGTC Symposium on Visualization (EuroVis '06), pp. 139–146, Lisbon, Portugal (2006)
[20] Theisel, H., Sahner, J., Weinkauf, T., Hege, H.C., Seidel, H.P.: Extraction of parallel vector surfaces in 3d time-dependent fields and application to vortex core line tracking. In: Proc. IEEE Visualization 2005, pp. 631–638 (2005)
[21] Theisel, H., Weinkauf, T., Hege, H.C., Seidel, H.P.: Saddle connectors - an approach to visualizing the topological skeleton of complex 3D vector fields. In: Proc. IEEE Visualization 2003, pp. 225–232 (2003)
[22] Theisel, H., Weinkauf, T., Hege, H.C., Seidel, H.P.: Topological methods for 2D time-dependent vector fields based on stream lines and path lines. IEEE Transactions on Visualization and Computer Graphics **11**, 383–394 (2005)
[23] Weinkauf, T.: Extraction of topological structures in 2d and 3d vector fields. Ph.D. thesis, Zuse Institute Berlin and Univ. Magdeburg, Informatik (2008)
[24] Weinkauf, T., Günther, D.: Separatrix persistence: Extraction of salient edges on surfaces using topological methods. Computer Graphics Forum **28**, 1519–1528 (2009)
[25] Weinkauf, T., Sahner, J., Günther, B., Theisel, H., Hege, H.C., Thiele, F.: Feature-based analysis of a multi-parameter flow simulation. In: Proc. SimVis 2008, pp. 237–251, Magdeburg, Germany (2008)
[26] Weinkauf, T., Sahner, J., Theisel, H., Hege, H.C.: Cores of swirling particle motion in unsteady flows. IEEE Transactions on Visualization and Computer Graphics **13**, 1759–1766 (2007)

[27] Weinkauf, T., Theisel, H., Hege, H.C., Seidel, H.P.: Boundary switch connectors for topological visualization of complex 3D vector fields. In: Data Visualization 2004. Proc. VisSym 04, pp. 183–192 (2004)

[28] Weinkauf, T., Theisel, H., Hege, H.C., Seidel, H.P.: Topological structures in two-parameter-dependent 2D vector fields. Computer Graphics Forum **25**, 607–616 (2006)